The Role of Aspartic Acid 143 in *E. coli* tRNA-Guanine Transglycosylase: Insights from Mutagenesis Studies and Computational Modeling

Katherine Abold Todorov, Xiao-Jian Tan, Susanne T. Nonekowski, George A. Garcia, and Heather A. Carlson
Department of Medicinal Chemistry, College of Pharmacy, University of Michigan, Ann Arbor, Michigan 48109-1065

ABSTRACT tRNA guanine transglycosylase (TGT) is a tRNA-modifying enzyme which catalyzes the posttranscriptional exchange of guanine in position 34 of $tRNA^{Y,H,N,D}$ with the modified base queuine in eukaryotes or its precursor, $preQ_1$ base, in eubacteria. Thus, TGT must recognize the guanine in tRNA and the free base queuine or $preQ_1$ to catalyze this exchange. The crystal structure of *Zymomonas mobilis* TGT with $preQ_1$ bound suggests that a key aspartate is critically involved in substrate recognition. To explore this, a series of site-directed mutants of D143 in *Escherichia coli* TGT were made and characterized to investigate heterocyclic substrate recognition. Our data confirm that D143 has significant impact on K_M of guanine; however, the trend in the K_M data (D143A < D143N < D143S < D143T) is unexpected. Computational studies were used to further elucidate the interactions between guanine and the D143 mutants. A homology model of *E. coli* TGT was created, and the role of D143 was investigated by molecular dynamic simulations of guanine bound to the wild-type and D143-mutant TGTs. To validate the model systems against our kinetic data, free energies of binding were fit using the linear interaction energy (LIE) method. This is a unique application of the LIE method because the same ligand is bound to several mutant proteins rather than one protein binding several ligands. The atomic detail gained from the simulations provided a better understanding of the binding affinities of guanine with the mutant TGTs, revealing that water molecules enter the active site and hydrogen bond to the ligand and compensate for lost protein-ligand interactions. The trend of binding affinity for wild-type > D143A > D143N > D143S > D143T appears to be directly related to the degree of hydrogen bonding available to guanine in the binding site.

INTRODUCTION

The modified base queuine (shown in Fig. 1) is found in the wobble position 34 of $tRNA^{Y,H,N,D}$ which exhibit the anticodon sequence GUN, where *N* represents any base (1). The queuine modification is present in virtually all eubacterial and eukaryotic organisms (2,3). Almost all modified bases are the results of chemical transformations of encoded/transcribed nucleotides (4); however, pyrrolopyrimidines like queuine are incorporated via an enzymatic transglycosylation reaction (5). The enzyme tRNA guanine transglycosylase (TGT) catalyzes the incorporation of $preQ_1$ base (7-aminomethyl-7-deazaguanine) into its specific tRNAs; it is further modified in situ to queuine (Fig. 1). In eukaryotic organisms, TGT incorporates queuine directly.

The *tgt* gene is found in many disease-causing bacteria including *Helicobacter pylori*, bacteria suspected to cause stomach cancer (6), and *Shigella flexneri*, bacteria which cause Shigellosis or ''bacillary dysentery''. The *Escherichia coli tgt* gene is homologous (>98% sequence identity) to the pathogenic *vacC* gene, which is known to be partially responsible for the virulent phenotype of *S. flexneri*. This has been demonstrated by the observation that an inactive *vacC*/*tgt* mutant exhibits a decrease in pathogenicity that is likely due to a decrease in bacterial invasion (7). Thus, TGT has become a novel target for antishigellosis therapy and possibly broad-spectrum antibiotics. The rational design of TGT inhibitors is an ongoing effort (8–11), and understanding the molecular recognition of substrates and inhibitors is important to these efforts.

Several key residues have been implicated as having vital roles in TGT activity due to their conservation in TGTs across species and kingdoms. Specifically, there are three aspartate residues in the TGT active site that are absolutely conserved among TGTs across all three kingdoms. Two of the aspartates (D89 and D264, *E. coli* TGT numbering) have been implicated in catalysis. TGT has been shown to go through a covalent enzyme-RNA intermediate, with one of the aspartates (initially thought to be D89 but now shown to be D264) acting as the enzymic nucleophile and the other aspartate (D89) acting as a general base (12–15). The third aspartate (D143) has been proposed to be involved in heterocyclic substrate recognition (16).

The crystal structure of $preQ_1$ bound to the *Zymomonas mobilis* TGT (16) reveals that D156 (equivalent of D143 in *E. coli* TGT) interacts with $preQ_1$ through hydrogen bonds to N-3 and the exocyclic amino group at C-2 (Fig. 2 *A*). The ping-pong kinetic mechanism of TGT (17) dictates that the wobble guanine of tRNA is bound in the $preQ_1$ binding

Submitted January 12, 2005, and accepted for publication May 27, 2005.

Address reprint requests to Heather A. Carlson, Dept. of Medicinal Chemistry, College of Pharmacy, University of Michigan, Ann Arbor, MI 48109-1065. Tel.: 734-615-6841; Fax: 734-763-2022; E-mail: carlsonh@umich.edu.

Katherine Abold Todorov's present address is Division of Forensic Toxicology, Armed Forces Institute of Pathology, 1413 Research Blvd., Bldg. 102, Rockville, MD 20850.

Susanne T. Nonekowski's present address is Dept. of Medicinal and Biological Chemistry, College of Pharmacy, The University of Toledo, 2801 West Bancroft St., Toledo, OH 43606-3390.

0006-3495/05/09/1965/13 $2.00

doi: 10.1529/biophysj.105.059576

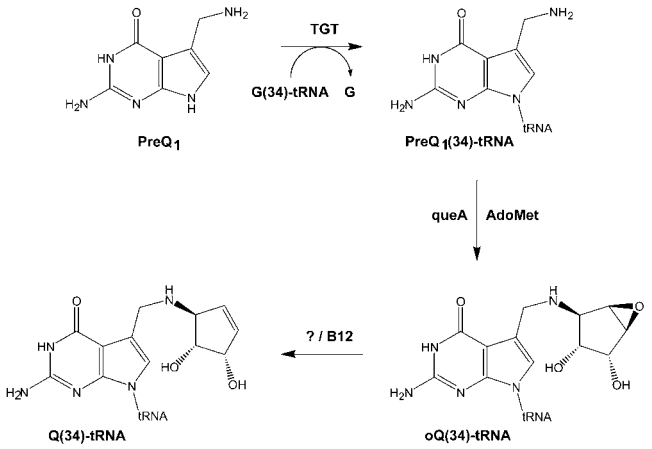

FIGURE 1 Biosynthesis of queuine-tRNA in eubacteria.

pocket, removed, and replaced with preQ$_1$. As such, the same active-site residues could be vital for recognizing guanine by making similar hydrogen-bonding contacts.

Romier et al. made two mutants of the equivalent of D143 in the *Z. mobilis* TGT (14). They found that both the alanine and tyrosine mutants were inactive. The crystal structures revealed that there was no change in the tertiary structure, ruling out a gross structural change as the cause of inactivity. Thus, the only experimental evidence to support a specific role in heterocyclic substrate recognition for D143 is the observation that these two mutants were inactive under the experimental conditions tested. However, these data are also consistent with a number of other roles for D143 (e.g., participation in catalysis, electrostatic stabilization of the transition state, or altered tRNA binding).

To more fully elucidate the role of D143 in the TGT reaction, this study has generated and characterized a series of mutants: D143A, D143N, D143S, and D143T. (We did not pursue the D143Y mutant because its inactivity appears to simply come from the increased steric bulk blocking the substrate's access to the active site.) Our four mutants were designed to probe various aspects of the hydrogen-bonding interactions of D143 with the heterocyclic substrate. Our data show that the mutants do not significantly alter the K_M of tRNA and have only a minor effect on k_{cat}—ruling out D143 being significant in the binding of tRNA or the rate-limiting catalytic step. Instead, K_M data for guanine show that D143 directly influences the binding of heterocycles.

However, we were surprised to find that the D143A mutant had the greatest affinity for guanine. The D143N mutant was expected to have the highest affinity for guanine, given its similarity to D143. Obviously, the activity of D143A points to a subtle and complex relationship. To interpret the trends observed in the experimental data, substrate recognition at the atomic level was explored with computer simulations. To achieve this, homology models of *E. coli* wild-type (wt) and D143-mutant TGTs were created based on the crystal structure of the *Z. mobilis* TGT (16). The models were then subjected to molecular dynamics (MD) simulations and free energy calculations using the linear

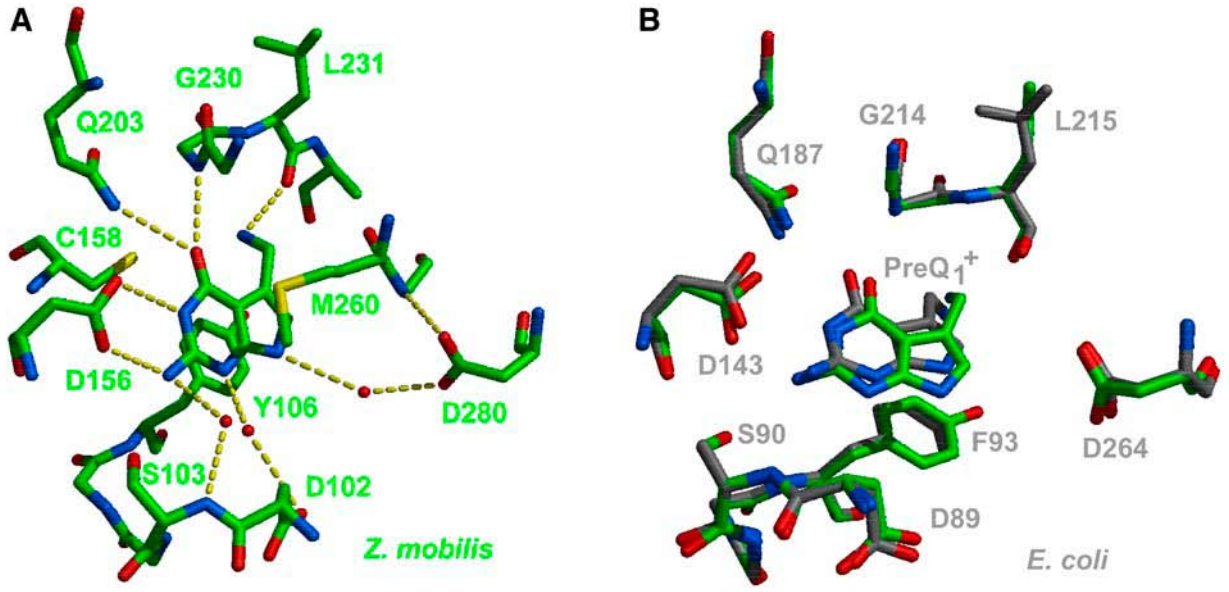

FIGURE 2 Comparison of the active sites of *Z. mobilis* TGT and our homology model of *E. coli* TGT. Structures are colored by atom type; the *Z. mobilis* structure has green carbon atoms, and the *E. coli* homology model has gray carbons. (*A*) The hydrogen-bonding pattern is given for the 2.2-Å crystal structure of *Z. mobilis* TGT with preQ$_1^+$ bound. (*B*) The fully energy-minimized homology model of *E. coli* TGT with preQ$_1^+$ is compared to the *Z. mobilis* crystal structure used in its creation. In the *E. coli* structure, bridging waters, the residues equivalent to *Z. mobilis* C158 and M260, and hydrogen atoms are not shown for clarity. The crystallographic waters and the cystiene and methionine residues were retained in the creation of the homology model, and their final positions were very similar to their initial locations.

interaction energy (LIE) method (18,19). Our models of the TGT system have assisted in the interpretation of the experimental data by providing details about the atomic interactions between the substrate (guanine) and enzymes (wt TGT and its D143 mutants).

METHODS

Determination of steady-state kinetic parameters for guanine and tRNA

His-tagged wt and mutant TGTs (htTGT(wt), htTGT(D143N), htTGT (D143T), htTGT(D143S), and htTGT(D143A)) were generated, expressed, and purified using standard techniques and materials (12) which are described in full detail in the Supplementary Material. Steady-state kinetic parameters (K_M and k_{cat}) for guanine and tRNA were determined for htTGT(wt) and the mutants using methodology previously described (20). The assays were performed, at least, in triplicate. htTGT (10 nM for wt and 50 nM for mutants) was incubated with various concentrations of tRNA and [^{3}H]-guanine in the presence of $MgCl_2$ (20 mM), DTT (5 mM), and HEPES, pH 7.3 (100 mM) in a total reaction volume of 400 μL. At varying intervals over an appropriate time course of 2–10 min or 15–120 min (longer time course for less active mutants), 70 μL aliquots were withdrawn and quenched in 2 mL of 5% TCA. The precipitated tRNA was then collected on Whatman GF/C filters. The filters were dried and counted via liquid scintillation. Initial velocities were obtained from linear regression of plots of pmol guanine (calculated from the measured DPM, the aliquot size, and the specific activity of the guanine used) incorporated versus time. The various enzyme concentrations were incorporated into the calculations, and concentrations of substrates were individually varied to obtain sets of initial velocities. To determine the guanine kinetic parameters for wt and all mutants, the tRNA concentration was held fixed at 20 μM. The guanine concentration ranges were: 0.05–20 μM, 0.25–250 μM, or 5–1000 μM depending on the mutant. To determine the tRNA kinetic parameters, the tRNA concentrations ranged from 0.1 to 40 μM with guanine fixed at 10 times its K_M for the particular mutant. Due to the lower specific activities of the TGT mutants, their time courses were lengthened to 120 min (15, 30, 60, 90, and 120 min intervals), and the concentrations of enzymes were increased to 50 nM. The initial velocities were plotted against the concentration of the varied substrate. Kinetic parameters (K_M and k_{cat}) were calculated from a nonlinear fit of the initial velocity data to the Michaelis-Menten equation. All kinetic parameters are calculated from the average of three replicate determinations of initial velocity data. All relative values were determined relative to htTGT(wt). The standard deviation within each point was calculated and is represented graphically by an error bar over each point in the data plots (21,22). The errors for the fitted parameters are standard errors of the fits (23).

Generation of the homology model of *E. coli* TGT

Additional parameters were required to model our heterocycles with the Amber94 force field (24). It was straightforward to generate these parameters using techniques outlined in the literature. The parameters and the complete details of their creation are provided in the Supplementary Material.

An alignment of *Z. mobilis* TGT and *E. coli* TGT sequences is provided in the Supplementary Material. There is 56% sequence identity and 68% sequence similarity between the two bacterial TGTs. The molecular modeling program MOE (25) was used to build the homology model of *E. coli* TGT with preQ$_1^+$ bound. A 2.2-Å crystal structure of *Z. mobilis* TGT with preQ$_1^+$ bound (R. Ficner, personal communication of coordinates, University of Marburg, Germany), was used as the basis for our *E. coli* model. Two short, unresolved loop regions (residues 99–106 and 115–124) were taken from the 1.8-Å, unbound structure of *Z. mobilis* TGT (Protein Data Bank (pdb) code 1PUD) (16,26). A three-residue deletion in the backbone (residues 190–192, *Z. mobilis* TGT numbering) was made at the end of a helical region exposed to solvent. Due to potential structural roles, all buried water molecules were kept.

The side chains in the *Z. mobilis* TGT structure were then altered to match the *E. coli* sequence starting at the binding site and working outward in successive shells retaining all common atom positions. Each new residue was manually checked for optimal hydrogen-bonding and electrostatic interactions. Ionization states of all ionizable groups were verified with pK_a calculations (27–29) using UHBD (30). No unusual ionization states were determined for typical acidic or basic side chains. All histidines were determined to be neutral, and the three cystienes that coordinate the zinc ion were determined to be deprotonated as expected. Both ends of the protein were capped because the *E. coli* TGT C-terminus is longer than the *Z. mobilis* TGT, and experimentally the *E. coli* TGT N-terminus is appended with a His·Tag. First the hydrogen atoms then the side chains of the *E. coli* TGT structure were energy minimized using the Amber94 force field within MOE (with our added parameters for preQ$_1^+$). Finally, the backbone was allowed to relax in the altered loop areas. The minimization protocol consisted of steepest descent steps to a root mean-square gradient of 10 kcal/mol·Å, conjugate gradient steps to a gradient of 1 kcal/mol·Å, and 200 truncated-Newton steps or a convergence of 0.001 kcal/mol·Å. Coordinates for the wt homology model are provided in the Supplementary Material.

MD simulations

All MD simulations and energy analyses were conducted using the Amber94 force field (24) and Sander_Classic from the AMBER6 (31,32) suite of programs. The nonbonded pair lists were updated every 20 steps. The van der Waals energies were truncated at a 10.0 Å distance; the electrostatic energies were truncated at 17.0 Å. The 1–4 electrostatic interactions and the 1–4 van der Waals interactions were divided by the scaling factors 1.2 and 2.0, respectively. PreQ$_1^+$ was replaced with guanine, and the homology model of *E. coli* TGT was hydrated with a 31-Å sphere of water centered on the bound ligand. The simulation of unbound guanine was also solvated in a 31-Å sphere of water. The chosen protocol followed appropriate standards in the field. Additional details are provided in the Supplementary Material for completeness.

The systems (wt TGT with guanine bound and guanine alone in solution) were equilibrated for 150 ps at a temperature of 310 K. At this point, the equilibrated wt TGT—with the altered loops relaxed and the active site adjusted to accommodate guanine—was modified to create mutant-TGT systems (residue D143 altered while conserving any analogous atomic positions). An additional 150 ps of equilibration was completed for the new mutant-D143 systems. After equilibration, 1 ns of sampling was completed with coordinates saved every 1.0 ps for structural and energetic analyses. Hydrogen-bonding analyses were carried out with AMBER's CARNAL program. Additional in-house codes were used to analyze bridging water molecules by measuring the distances and angles to define multiple hydrogen bonds. The required distance for a hydrogen bond was 3.5 Å or shorter between the heavy atoms (3.7 Å or less for hydrogen bonds involving sulfur atoms). The *X-H-Y* angles were required to be 120–180°.

Free energies calculated using the LIE method

The LIE method (Eq. 1), developed by Åqvist and coworkers (18), samples the ligand in explicit solvent alone and bound to protein. Free energies are then estimated by a comparison of the energetics of the ligand in those two environments. The interactions between the ligand and its environment (either pure solvent or protein with solvent) are divided into electrostatic (ΔG_{elec}) and van der Waals (ΔG_{vdw}) components. The binding free energy (ΔG_{bind}) is estimated as

$$\Delta G_{bind} = \Delta G_{elec} + \Delta G_{vdw} \cong \frac{1}{2}(\langle E_{elec}\rangle_{bound} - \langle E_{elec}\rangle_{free}) + \alpha(\langle E_{vdw}\rangle_{bound} - \langle E_{vdw}\rangle_{free}), \quad (1)$$

where $\langle E_{elec} \rangle$ and $\langle E_{vdw} \rangle$ are the average electrostatic and van der Waals interaction energies of the ligand with its environment, and the bound and free subscripts refer to simulations of the ligand bound to the protein or alone in explicit solvent, respectively. Each energetic value is an average taken from the ensemble of configurations generated by MD. In Eq. 1, the electrostatic scaling factor of 1/2 is a standard value derived from statistical mechanics. The van der Waals scaling factor, α, is dependent on the protein system; other groups have reported values ranging from 0.1 to 1.2 for various protein systems (18,19,33–43).

The electrostatic and van der Waals energies of the ligand with its environment were provided by Sander_Classic (which we modified to print the necessary energetic components). The values were determined for each MD snapshot, and the energetic components were averaged to obtain E_{elec} and E_{vdw} for both bound and free systems.

The binding free energy (ΔG_{bind}) was estimated using the LIE method (Eq. 1). It is necessary to determine an appropriate value for α based on the experimental data for guanine and TGT (wt, D143A, D143N, D143S, and D143T). The average energies were RMS fit to the experimental data to determine the most appropriate value for α. Below, the reasonable value for α and the accurate trend in ΔG_{bind} indicate that the simulations and methodology are appropriate to provide insight into this system.

RESULTS AND DISCUSSION

Determination of steady-state kinetic parameters for guanine and tRNA

A series of D143-mutants of TGT was generated to investigate the role of this residue, postulated to involve heterocyclic substrate recognition. The various mutations were designed to probe the hydrogen-bonding contacts between this residue and the N-3 and the exocyclic amine at C-2 of the heterocyclic substrate. The htTGT(D143N) mutation removes one hydrogen-bond acceptor (substituting it with a potential hydrogen-bond donor, the amide nitrogen). The htTGT(D143T) mutation also removes one hydrogen-bond acceptor and displaces the remaining hydrogen-bond acceptor (also a possible donor) by one methylene group but incorporates some potential van der Waals contacts via the methyl group. The htTGT(D143S) mutation has the same hydrogen-bonding capability as the threonine mutant but lacks the potential van der Waals contacts of the methyl group. Lastly, the htTGT(D143A) mutation removes the possibility for any hydrogen bonds, and its small size provides little, if any, van der Waals contacts.

The mutant TGTs (except for D143T) were originally constructed and found to overexpress only in the presence of chromosomally encoded, wt TGT. This strongly suggests a significant role for D143. It is attractive to speculate that if D143 is involved in heterocyclic substrate recognition, then the mutants may allow ''incorrect'' bases to be incorporated into the TGT-substrate tRNAs. This would result in tRNAs with altered anticodons, leading to loss of fidelity during translation at the ribosome and, ultimately, cell death. The presence of the higher-activity, wt TGT would ''protect'' the tRNAs by correctly modifying them and doing so more efficiently than the mutants with their poorer catalytic activity.

The kinetic parameters for all TGTs have been determined for tRNA (Table 1) and for guanine (Table 2) using the guanine exchange assay. htTGT(wt) shows kinetic parameters comparable (within a factor of 2–3) to those of wt TGT (Tables 1 and 2), indicating that the His·Tag does not significantly perturb TGT activity. The hyperbolic plots obtained from fitting the initial velocity data versus substrate concentration to the Michaelis-Menten equation are shown in Fig. 3 for htTGT(wt), htTGT(D143A), htTGT(D143N), htTGT(D143S), and htTGT(D143T). On each plot is an inset of the low concentration range to better depict visually how well the data fit to the Michaelis-Menten equation.

A direct role for D143 in catalysis would predict a large decrease in k_{cat} values for the D143 mutants; however, only a 4- to 16-fold reduction in k_{cat} is observed compared to htTGT(wt). In contrast, the k_{cat} values of TGT(D89) mutants are reduced ~100- to 1000-fold compared to wt (12). Additionally the k_{cat} values for all D143 mutants are almost identical to one another. This modest and consistent decrease in activity suggests that the mutations are not directly affecting catalysis. It is possible that some indirect effects may be responsible for this small effect on catalysis (further discussion below).

A significant role for D143 in binding tRNA would predict a change in K_M for tRNA in the D143 mutants relative to wt; however, this also is not observed. In fact, the K_M values for tRNA are very similar (~1.5- to 3-fold different) for the mutants relative to wt, with a range of K_M values from 0.6–1.9 μM. Our current models of the kinetic (17) and chemical

TABLE 1 Table of tRNA kinetic parameters for TGTs

Enzyme	k_{cat}*†‡ ($10^{-3}s^{-1}$)	K_M*†‡ (μM)	k_{cat}/K_M*†‡ ($10^{-3}s^{-1}\mu M^{-1}$)	Relative K_M*‡§	Relative k_{cat}/K_M*‡§
TGT(wt)¶	5.2 (0.3)	0.19 (0.05)	27 (7)	–	–
htTGT(wt)	3.10 (0.09)	0.60 (0.09)	5.1 (0.8)	1.0	1.0
htTGT(D143A)	0.36 (0.18)	0.83 (0.08)	0.43 (0.22)	1.4	0.084
htTGT(D143N)	0.56 (0.02)	1.5 (0.3)	0.36 (0.06)	2.6	0.071
htTGT(D143S)	0.27 (0.01)	1.9 (0.3)	0.15 (0.02)	3.2	0.029
htTGT(D143T)	0.20 (0.02)	1.8 (0.3)	0.11 (0.02)	3.0	0.022

*Errors are shown in parentheses.
†Kinetic parameters are calculated from the average of three replicate determinations of initial velocity data.
‡Error was calculated as detailed in the methodology and referenced in Gordon and Ford (21) and Harris (22).
§Relative values were determined relative to that of His-tagged wt.
¶TGT (wt) data were taken from Goodenough-Lashua (54).

TABLE 2 Table of guanine kinetic parameters for TGTs

Enzyme	k_{cat}*†‡ ($10^{-3}s^{-1}$)	K_M*†‡ (μM)	k_{cat}/K_M*†‡ ($10^{-3}s^{-1}\mu M^{-1}$)	Relative K_M*‡§	Relative k_{cat}/K_M*‡§
TGT(wt)¶	6.3 (0.1)	0.35 (0.03)	18 (2)	–	–
htTGT(wt)	2.3 (0.1)	0.15 (0.02)	16 (2)	1.0	1.0
htTGT(D143A)	0.38 (0.01)	11 (1)	0.033 (0.003)	75	0.0022
htTGT(D143N)	0.58 (0.02)	22 (3)	0.027 (0.003)	145	0.0017
htTGT(D143S)	0.25 (0.01)	57 (8)	0.0044 (0.0007)	380	0.00028
htTGT(D143T)	0.20 (0.01)	105 (22)	0.0019 (0.0004)	700	0.00012

*Errors are shown in parentheses.
†Kinetic parameters are calculated from the average of three replicate determinations of initial velocity data.
‡Error was calculated as detailed in the methodology and referenced in Gordon and Ford (21) and Harris (22).
§Relative values were determined relative to that of His-tagged wt.
¶TGT (wt) data were taken from Goodenough-Lashua (54).

mechanisms (12,13) for TGT suggest that D143 interacts with G-34 of tRNA. However, given the number of interactions that must exist in the interface between tRNA and TGT, it is reasonable to find that changes in the D143-G-34(tRNA) interaction have a minimal effect on the K_M of the whole tRNA.

The greatest impact that the mutations have on the kinetics of the TGT reaction involves the K_M of guanine. An ~75-fold increase (relative to wt) is observed in the K_M value for htTGT(D143A); a 150-fold for htTGT(D143N); a 380-fold increase for htTGT(D143S) and a 700-fold increase for htTGT(D143T) is seen. A similar, but decreasing, trend for k_{cat}/K_M is seen for the mutants; however, the magnitude is larger with a range for the mutants of 450- to 8300-fold decrease in k_{cat}/K_M relative to wt. The slight and consistent decrease in k_{cat} (10-fold) for the mutants indicates that this decreasing trend in catalytic efficiency (k_{cat}/K_M) is due almost exclusively to the increase in K_M for guanine. It should be noted that, in general, K_M is not a true dissociation constant. As mentioned above, the kinetic mechanism for TGT-catalyzed guanine exchange is ping-pong, with tRNA binding first. However, it is very likely that the rate-limiting step occurs after guanine binds to the TGT-tRNA covalent intermediate (44). If this is the case, then the K_M values reported here for guanine should closely approximate (if not equal) the dissociation constants for guanine and can be treated as such.

The dramatic change in K_M values for guanine upon mutating D143 supports the hypothesis that its primary role is the recognition of heterocycles in the catalytic site. It was reasonable to assume that the K_M values for guanine would have increased in this order: wt < D143N < D143T < D143S < D143A due to each protein's potential for forming hydrogen bonds with guanine. However, the results yield an overall trend in guanine K_M of wt < D143A < D143N < D143S < D143T. We observe a similar trend in decreasing catalytic efficiency (k_{cat}/K_M). The fact that htTGT(D143A) has a lower guanine K_M value than the other mutants seems counterintuitive. Mutation of aspartate to alanine removes the possibility of any hydrogen bonds between residue 143 and the heterocyclic substrate, whereas at least one potential hydrogen bond remains with each of the other mutants. To explore the possible causes of the unexpected trend, we used MD simulations to provide atomic details of the recognition between guanine and each TGT system.

Simulating the guanine-TGT system

The eubacterial TGT is a bisubstrate enzyme, binding both tRNA and a heterocycle. The experimental binding data were determined in the presence of tRNA. However, no crystal structures existed for TGT bound to RNA until after our calculations were complete. The first and only cocrystal structure was an RNA minihelix covalently attached to the *Z. mobilis* TGT (15). Still, no crystal structures exist of a full tRNA bound to any TGT, and no crystal structures exist for any *E. coli* TGT systems.

For our calculations, docking tRNA (and its many counterions) to TGT to create a TGT·tRNA complex would have introduced too much uncertainty into our models. We chose to study TGT and the heterocycle without bound tRNA. Though this is a simplification of the real system, the point of this study is to clarify the role of D143, and it appears that tRNA is not a significant factor for D143 for several reasons.

First, the structure was unchanged by binding RNA (15). The crystal structure of *Z. mobilis* TGT bound with the RNA minihelix clearly indicates that no structural changes occur in the active site of TGT upon RNA binding.

Second, residue 143 most likely has the same interactions to the heterocycle with or without tRNA. In the $preQ_1^+ \cdot$ TGT structure (16), D143 binds to the aminopyrimidone portion of $preQ_1^+$ at a point that is distal to where the body of the tRNA is likely to bind.

Third, the interaction of tRNA with TGT·heterocycle is expected to be the same for all mutants. This is supported by the observation that residue D143 seems to have very little overall effect on the binding of tRNA (evidenced by the K_M values of D143 mutants with tRNA in Table 1). Because the interaction of RNA with all TGTs is the same, leaving the tRNA out of the model is a constant, systematic simplification. If the simplification is consistent across all the simulations, the LIE methodology can correct for the missing

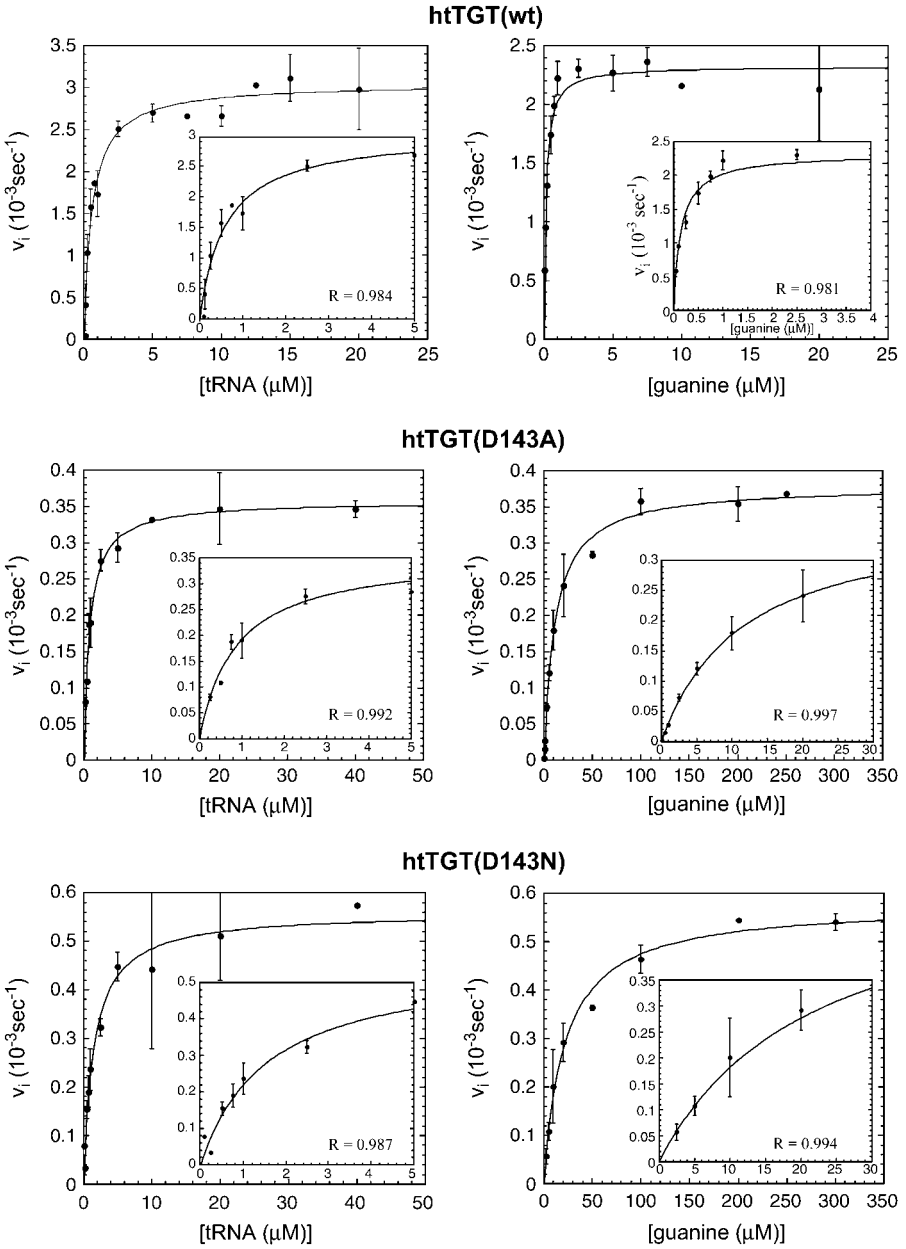

FIGURE 3 Wt and D143-mutant TGT data fit to Michaelis-Menten kinetics. (*Left*) tRNA. (*Right*) Guanine. Curves were obtained from the average of three independent determinations of initial velocity data. Error bars are generated from the standard deviation in each point. The insets are expansions of the low concentration ranges.

tRNA in the free energy calculations. The systematic error is compensated by the fitting of α for the system.

Lastly, these calculations were done in close collaboration with the experimental studies. The agreement between the experimental and computational data supports our models. Without the consistency of the data and the collaboration between the research groups, developing simplified and reliable models would have been too risky.

The LIE method is also appealing because it is 5–10 times faster than free energy perturbation calculations (35). Though LIE is less accurate than free energy perturbation, it still accounts for the flexibility of proteins by employing either MD or Monte Carlo sampling. LIE also incorporates the unbound state of the ligand to account for binding penalties such as desolvation. This makes the LIE method attractive for our studies and structure-based drug design (33–35). It should be noted that generalized Born/surface area and Poisson-Boltzmann/surface area methods are also popular for estimating binding free energies (39,45–48), but they are computationally more expensive and no more accurate than LIE. They cannot be used in this study because the missing tRNA would greatly alter the electrostatics calculations at the heart of those methods, and there is no way that we can compensate for the missing tRNA as we can with LIE. Furthermore, these methods require estimates of the entropic contributions based on normal mode analysis, but these will also be incorrect without tRNA.

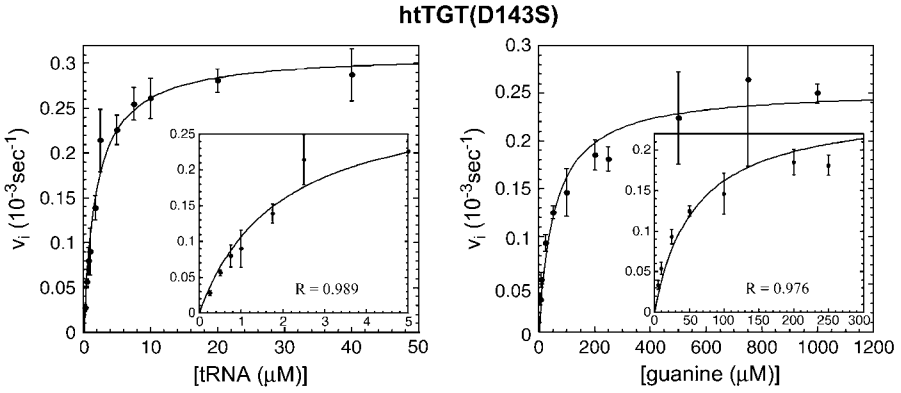

FIGURE 3 Continued.

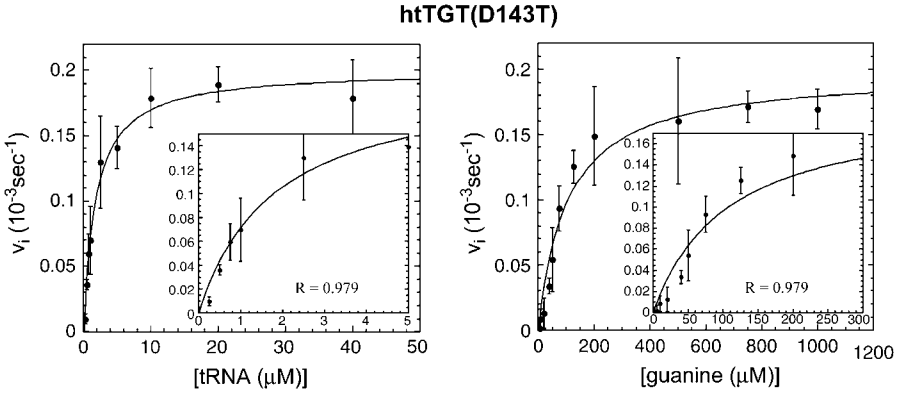

Reliability of the homology model

A homology model of *E. coli* TGT was created to answer key recognition questions involving residue D143. The 2.2-Å crystal structure of *Z. mobilis* TGT with $preQ_1^+$ bound was used as the starting structure for the homology model. The sequence alignment given in the Supplementary Material shows that the *Z. mobilis* structure is a good basis for the *E. coli* model. Also, the reliability of the resulting homology model is highlighted by its structural similarity to related systems. Fig. 2 *B* shows the similarity of the active sites of the *Z. mobilis* TGT·$preQ_1^+$ complex and the fully energy-minimized homology model of *E. coli* TGT with $preQ_1^+$ bound (the model before solvation and changing the ligand to guanine). Only a slight shift in the location of $preQ_1^+$ is seen, and the homology model is in good agreement with the crystal structure used in its creation. It is also similar to another related structure; Xie et al. were able to soak 9-deazaguanine into a *Z. mobilis* TGT complex (15). The aspartate that corresponds to D143 makes the same two key hydrogen bonds to 9-deazaguanine that are seen in the $preQ_1^+ \cdot$ TGT structure and the homology model.

It is interesting to note that our model of wt *E. coli* TGT binding guanine shows similar hydrogen bonds to those that are seen in an archaeosine TGT crystal structure (49), providing a second independent validation that the simulations are accurate. A crystal structure of an archaeal TGT with guanine bound shows that the D130 (analogous to D143 in *E. coli* TGT) makes two hydrogen bonds with N-1 and the exocyclic amine of guanine; Q196 (analogous to Q187 in *E. coli* TGT) and G214 (as opposed to C145 in *E. coli* TGT) are also within hydrogen-bonding distance to the oxygen of guanine. Possible base stacking of guanine with F93 is also seen. A common hydrogen-bonding pattern is expected due to the conservation of key active-site residues which are presumably responsible for binding the common substrate.

Temperature, total energy, total potential energy, and potential energy components (electrostatic and van der Waals energies) showed that all five systems were fully equilibrated after 150 ps of sampling at 310 K. The following 1-ns sampling phase generated ensembles of conformations from which structural and energetic analyses were performed. Structural analyses of the protein conformations obtained from each picosecond of the protein-ligand simulations showed no marked difference to their initial structures. Of course, regions of the system $\geq$24 Å from the center of guanine were restrained because of our use of a 31-Å sphere of water to solvate the system. However, the average RMSD of the mobile region of the protein was modest and appropriate, only 1.05 Å from its starting structure. Furthermore, the modified loop regions, which were fully flexible in the simulation and the most likely to exhibit altered structure, did not change significantly. This indicates stable homology models and properly executed MD simulations.

TABLE 3 Energy components of guanine interacting with TGTs, in kcal/mol

Enzyme	$\langle E_{elec}\rangle^{*}_{bound}$	$\langle E_{vdw}\rangle^{*}_{bound}$	$\langle E_{elec}\rangle_{bound} - \langle E_{elec}\rangle^{\dagger}_{free}$	$\langle E_{vdw}\rangle_{bound} - \langle E_{vdw}\rangle^{\ddagger}_{free}$
Wild-type	−57.0	−22.7	−7.4	−11.8
D143A	−47.7	−24.1	1.9	−13.2
D143N	−48.4	−23.1	1.2	−12.2
D143S	−47.7	−23.2	1.9	−12.3
D143T	−47.9	−23.7	1.7	−12.8

*Energies are an average of 1000 energies taken from the sampling run.
†The average electrostatic energy of free ligand in water is −49.6 kcal/mol.
‡The average van der Waals energy of free ligand in water is −10.9 kcal/mol.

Energy analysis and free energies of binding

Sander_Classic was modified to report the energy components between the ligand and its environment. Table 3 shows the average values for electrostatic and van der Waals energies for guanine interacting with TGT and water. Because all binding events are in equilibrium with an unbound state, the energies from the MD simulations of the unbound ligand must be subtracted from the energies in the bound state in the LIE methodology (Eq. 1). These values are also given in Table 3. To show the convergence of these values, plots of E_{vdw}, E_{elec}, $\langle E_{vdw}\rangle$, and $\langle E_{elec}\rangle$ versus time are provided in the Supplementary Material.

There are very few experimentally determined binding constants for TGT due to the nature of the experimental assay system and the difficulty in obtaining radio-labeled substrates. As discussed above, the kinetic mechanism for TGT and other observations strongly suggest that the K_M for guanine closely approximates, and may actually be equal to, the dissociation constant for guanine. Therefore, the experimentally measured K_M values of guanine with TGT (wt and D143 mutants) were used to estimate K_A in determining an experimental value for ΔG_{bind} for each system (Table 4). An α value of 0.55 ($\pm$ 0.04) was obtained by an RMS fit to the experimental data for all five TGT systems. The experimentally fit scaling factor provided the calculated free energies of binding (Table 4). Plots showing the convergence of ΔG_{bind} over the MD simulations are provided in Supplementary Material. The later halves of the MD simulations show little drift (<1 kcal/mol) in the calculated values.

The experimental values for ΔG_{bind} were well reproduced, which helps validate the appropriateness of the model, the stability of the MD simulations, and the fit of the scaling factor α. The order of ΔG_{bind} is correct except for D143T, and given the small range in free energies of binding, this agreement is very good. Also, the low activity of the D143S and D143T mutants resulted in larger errors in their K_M values (~20% for D143T), so reproducing these values is expected to be more difficult.

Given that the calculated free energies are in good agreement with the experimental data, it would appear that the LIE method was capable of compensating for the simplification of the computational model. The value of 0.55 for α is well within the range of the values reported in the literature (0.1–1.2). An unusual value was not necessary to compensate for the omission of tRNA in the model. This homology model should be useful and accurate for examining the molecular recognition of similar heterocycles to TGT and the D143-mutant TGTs.

TABLE 4 Comparison of experimental and LIE free energies of guanine of binding to TGTs

Enzyme	Experimental* ΔG_{bind} (kcal/mol)	Calculated† ΔG_{bind} (kcal/mol)	Difference in ΔG_{bind} (kcal/mol)
Wild-type	−9.7	−10.2	−0.5
D143A	−7.0	−6.3	0.7
D143N	−6.6	−6.1	0.5
D143S	−6.0	−5.8	0.2
D143T	−5.6	−6.2	−0.6

*ΔG_{bind} = –RT (ln K_A), where K_A is estimated as equal to $(K_M)^{-1}$ as reported in Table 2.
†Based on Eq. 1, the energies in Table 3, and a van der Waals scaling factor, α, of 0.55 ($\pm$0.04).

Structural analysis of wt and mutant TGTs

Hydrogen bonds are an important aspect of recognition between TGT and its ligands. Fig. 4 depicts the hydrogen-bonding schemes observed for guanine with wt and D143-mutant TGTs. Because wt TGT is proposed to recognize both guanine and $preQ_1^+$ in the same site, it is interesting to compare the hydrogen-bonding patterns of guanine bound to wt in Fig. 4 to $preQ_1^+$ bound to wt in Fig. 2 *B*. The major difference between $preQ_1^+$ and guanine is the charged amino-methyl group of $preQ_1^+$. During the MD, the smaller guanine ligand has shifted deeper into the active site of wt TGT, placing the five-membered ring into the region occupied by the amino-methyl group of $preQ_1^+$. This provides a slightly different hydrogen-bonding pattern. The shift moves guanine away from its van der Waals contact with the side chain of M244, but this allows the backbone of M244 to accept a hydrogen bond from guanine in the wt simulation. Also, the hydrogen bond made by the backbone of G214 in initial homology model was replaced by a partial hydrogen bond from the C145 side chain in the MD (*Wild type* in Fig. 4, but it should be noted that all of the D143 mutants exhibit a hydrogen bond between G214 and guanine).

To understand the differences in binding between the wt and mutant TGT, it is important to compare the patterns of molecular recognition. Table 3 shows that the major difference between the wt and D143-mutant TGTs is the electrostatic interaction energy. The strong electrostatics comes from the hydrogen bonds between guanine and the charged side chain of D143. The complementarity is very specific and tight. This is also obvious in the MD because the conformational sampling of guanine within the binding site is limited (data not shown).

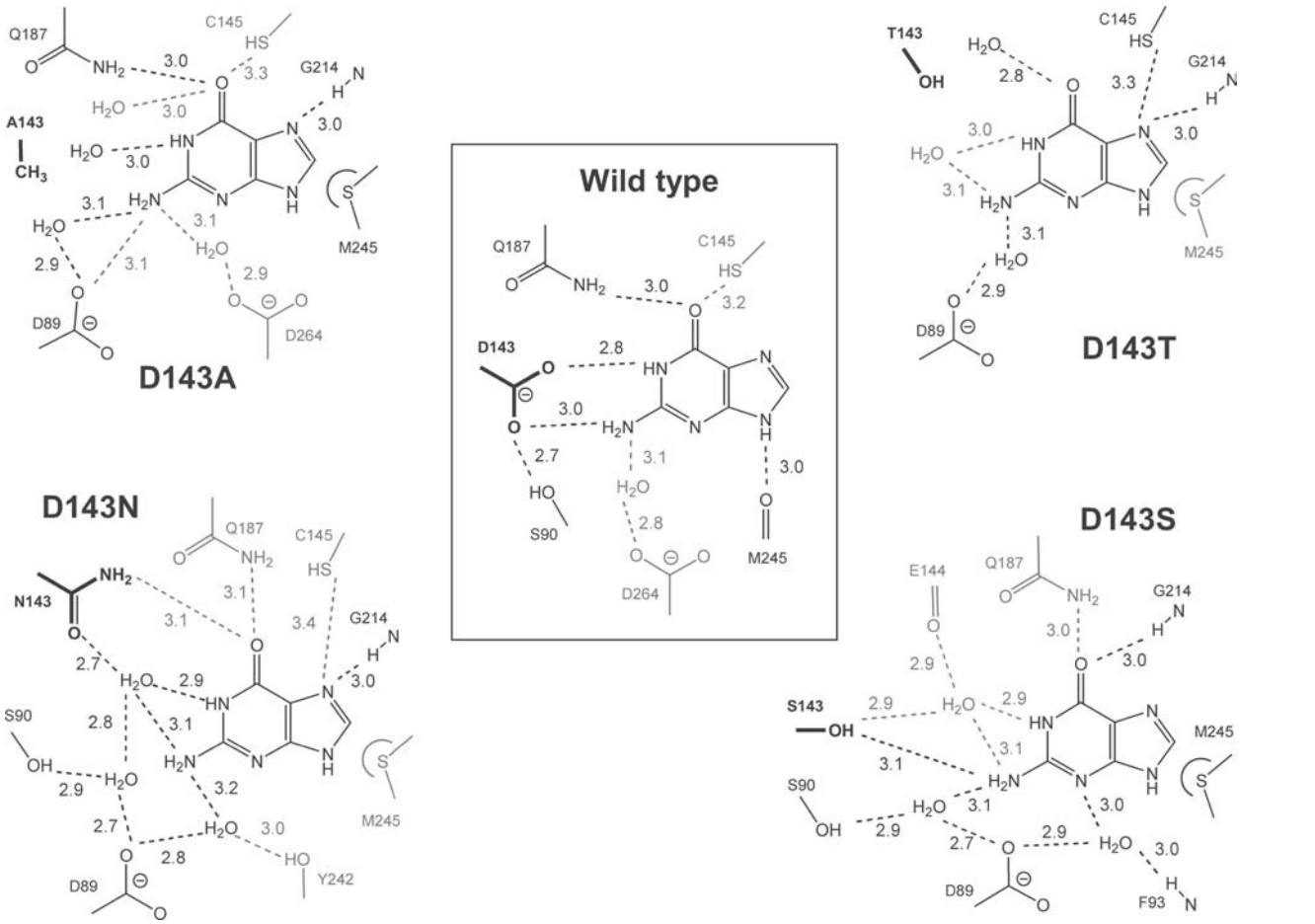

FIGURE 4 Hydrogen-bonding schemes for guanine bound to wt and D143-mutant TGTs. Distances are given in Ångstroms. Interactions shown in black are observed in 72–100% of the snapshots from the MD; interactions in gray are observed in 40–67% of the snapshots. Details of the occupancy for each interaction are given in the Supplementary Material.

The similarity in the experimental free energies of binding in Table 4 implied that the differences between the mutants would be more subtle. Table 3 confirms this because the energy components for all mutants fall within a 1 kcal/mol range. Our greatest interest was to explain the unexpected K_M trend—why did the D143A mutant have the tightest binding affinity? We were surprised to find an elaborate network of water molecules that bridge between the binding site and the guanine ligand (Fig. 4). The D143A simulation has more bridging waters than what is seen in Fig. 2 *A*, but several positions are similar. Another similarity to Fig. 2 *A* is the fact that D89, S90, and D264 are important in orienting the bridging water in many of the mutants. Table 5 shows that the water molecules actually permit the D143A mutant to provide the most hydrogen bonds to complement guanine. This network was highly mobile with several exchanging water molecules that continued to provide the same large number of hydrogen bonds to guanine. Water has also been seen to compensate for a mutation of aspartate to asparagine in hypoxanthine phosphoribosyl transferase (HPRT) (50).

TABLE 5 Number of hydrogen bonds between guanine and the TGT binding sites

	Ligand-protein hydrogen bonds		Water-mediated hydrogen bonds		Total hydrogen bonds		Experimental ΔG_{bind}
Enzyme	Full	Partial	Full	Partial	Full	Partial	(kcal/mol)
Wild-type	4	1	0	1	4	2	−9.7
D143A	2	2	2	2	4	4	−7.0
D143N	1	3	3	0	4	3	−6.6
D143S	2	1	2	2	4	3	−6.0
D143T	2	0	2	2	4	2	−5.6

Crystal structures of the HPRT mutant D137N reveal that several water molecules mediated hydrogen bonds between the ligand and the protein side chains.

Table 5 also shows that the number of hydrogen bonds for the mutants parallel the experimental free energies of binding. As one would expect, a greater number of hydrogen bonds by the side chains and bridging water molecules provides a tighter complement and stronger free energies of binding (D143A > D143N > D143S > D143T). Though the calculated free energy of binding is out of order for D143T in Table 4, the patterns observed in the MD parallel the experimental data. The hydrogen-bonding pattern seen for D143T shows the least number of hydrogen bonds—providing little water-mediated rescue of recognition—appropriate for D143T having the poorest K_M. Also, the movement of guanine in the binding site during the MD is significant, showing poor complementarity (data not shown). As mentioned earlier, the larger error in the K_M values for D143T may explain why its calculated free energy of binding is out of order.

Additional patterns in the simulations of all mutant TGTs may also explain part of their reduced binding affinity for guanine. In the original *Z. mobilis* structure and *E. coli* homology model with $preQ_1^+$, D143 and S90 are ~4 Å apart and do not share a hydrogen bond, but the simulations revealed an important secondary role for D143 and S90. In the simulations of wt *E. coli* TGT with guanine, S90 and D143 make a strong hydrogen bond (average O-O distance of 2.7 Å and average O-H-O angle of −175.8° between the hydroxyl group of S90 and the carboxylate group of D143). In the mutants, loosing the aspartate removes this hydrogen bond and causes S90 to adopt a conformation away from residue 143 (moving ~2 Å, Fig. 5) to a position more similar to that seen in the *Z. mobilis* crystal structure. Others have proposed that S90 is used to orient the substrate (11,51), but the distance observed between the ligand and S90 in the simulations and the crystal structure is too long for a proper hydrogen bond. In the farther position seen in the MD of the mutants, S90 is able to coordinate bridging water molecules to complex guanine as noted above.

In the mutants, changes are also seen in D264 and M244-V246. D264 twists 90°. The twist helps D264 and neighboring Y242 to interact with bridging water in the binding site. D264 and Y242 play a direct role with bridging water in the D143A and D143N simulations, respectively (Fig. 4). Also, D264 is known to orient bridging water molecules in crystal structures of *Z. mobilis* TGT (13). Although water bridging between D264 and the heterocycle is interesting, it should be noted that D264 performs a nucleophilic attack during catalysis. This is its primary function, and we do not want to overemphasize any role it may play in the recognition of guanine.

The reorientation of D264 breaks its hydrogen bond with the backbone of G245 that is seen in the wt simulation (important for D264 to be available for the nucleophilic attack). G245 moves, but more importantly, this changes the positions of neighboring M244 and V246 (Fig. 5). M244 moves ~1.5 Å. This breaks the hydrogen bond between guanine and the backbone of M244, and instead, there is an interaction between guanine and the side chain in a van der Waals, sulfur-aromatic interaction only seen in the mutants (or in the wt binding $preQ_1^+$). V246 flips its side chain significantly, and this makes A216 and V217 move down to fill missing van der Waals interactions. This change in the shape of the pocket due to A216, V217, V246, and M244 may account for the slightly greater van der Waals interaction energies in the mutants (Table 3).

The backbone of residues 213–217 becomes highly mobile in response to the movement of V246. A216 and V217 respond as noted above, and the peptide bond between

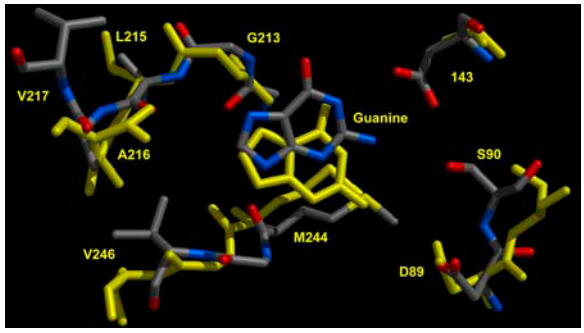

FIGURE 5 Average structures from the simulations of wt and D143A TGT highlight the changes observed in many of the active site residues. Large shifts are seen for guanine, S90, A216, V217, and V246. More mild changes are seen in G213, L215, and M244. Wt is colored by atom type, and D143A is in yellow.

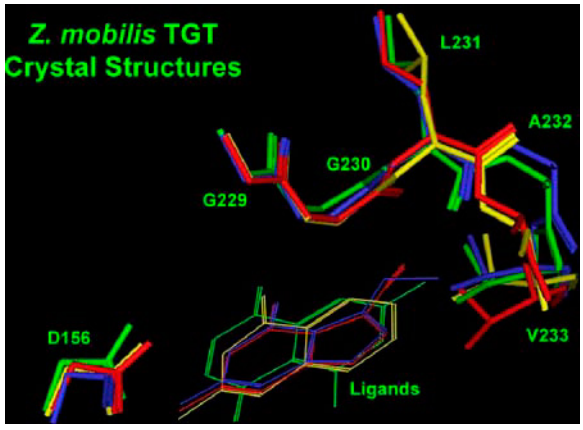

FIGURE 6 Flexibility in the 213–217 region of *E. coli* TGT is seen in the same region of *Z. mobilis* TGT (residues 229–233). The examples shown are from crystal structures of *Z. mobilis* TGT with different ligands bound: $preQ_0$ (7-deaza-7-cyano-guanine) is shown in red (PDB code 1P0B, (53)); $preQ_1$ (7-deaza-7-aminomethyl-guanine) is blue (PDB code 1P0E, (53)); 3,5-diaminophthalhydrazide is green (PDB code 1F3E, (52)); 2-amino-quinazolin-4(3H)-one is yellow (PDB code 1S39, (10)).

G213 and G214 flips its backbone by 90°. Fig. 6 shows how this same region in *Z. mobilis* TGT rearranges the backbone in response to binding different heterocyclic ligands. Though this region appears to have a higher degree of flexibility than one might expect, it inherently adapts to changes in the binding site whether caused by mutation or binding different ligands.

CONCLUSION

Our experimental studies have shown that *E. coli* D143-mutant TGTs have reduced activity due to altered binding of heterocycles with only a very minor reduction in catalysis and no discernable effect on tRNA binding. Due to the absolute conservation of this residue in TGTs across kingdoms, it is reasonable to propose that D143 carries out this role in all TGTs. We were surprised to find that the D143A mutant exhibited a higher affinity for guanine than D143N, D143S, and D143T. Hydrogen-bonding arguments would imply that D143A have the poorest affinity. To understand this trend, we turned to computer models of TGT.

Our homology model gave us insight into the experimental results. The model was validated by its similarity to related systems and its ability to accurately reproduce free energies of binding based on MD simulations. It was possible to fit the van der Waals scaling factor, α, to the experimental data yielding a value of 0.55; this value is well within the literature established values of 0.1–1.2. The LIE method has been successfully used throughout the literature to predict free energies of binding, generally to rank many ligands binding to one receptor. It is important to note that this is one of the few examples of the successful prediction of a single ligand binding to multiple mutant enzymes.

Several patterns have been observed in the MD to explain the differences in binding between the wt and mutant TGTs. The high binding affinity seen in the wt TGT is due to strong hydrogen bonding and good electrostatics between guanine and the charged side chain of D143. The unexpected low K_M value seen for D143A appears to be caused by several water molecules entering the active site and providing bridging hydrogen bonds between the ligand and binding site, thereby compensating for lost protein-ligand interactions. The reduced binding affinity for the mutants (D143A $>$ D143N $>$ D143S $>$ D143T) appears to be due to lost hydrogen bonds and poorer molecular recognition.

Many of the bridging water molecules are held in proper orientation by D89, S90, and D264. The loss of the carboxylate at D143 allows S90 and D89 to reorient and play this important new role. Additional changes are also observed in the conformation of D264 and M244-V246 that allow for new binding motifs. Lastly, the backbone from G213-V217 is highly mobile and adaptive. This is in agreement with recent crystal structures of *Z. mobilis* TGT (10,52,53).

SUPPLEMENTARY MATERIAL

An online supplement to this article can be found by visiting BJ Online at http://www.biophysj.org.

We thank Dr. Jeff Kittendorf and Dr. C. Eric Thomas for critical review of the experimental procedures and results reported in this manuscript. We also thank Dr. Ralf Ficner (University of Marburg, Germany; present address: Max-Planck Institute, Göttingen, Germany) for the personal communication of crystal structure coordinates.

This work was supported in part by the National Institutes of Health (GM65372, H.A.C.; GM065489, G.A.G.) and the University of Michigan, College of Pharmacy, Vahlteich Research Fund (G.A.G.). K.A.T. acknowledges the support of the Chemistry-Biology Interface Training Program (GM08597).

REFERENCES

1. Harada, F., and S. Nishimura. 1972. Possible anticodon sequences of $tRNA^{His}$, $tRNA^{Asn}$, and $tRNA^{Asp}$ from *Escherichia coli* B. Universal presence of nucleoside Q in the first position of the anticodons of these transfer ribonucleic acids. *Biochemistry*. 11:301–308.
2. Grosjean, H., M. Sprinzl, and S. Steinberg. 1995. Posttranscriptionally modified nucleosides in transfer RNA: their locations and frequencies. *Biochimie*. 77:139–141.
3. Kasai, H., Y. Kuchino, K. Nihei, and S. Nishimura. 1975. Distribution of the modified nucleoside Q and its derivatives in animal and plant transfer RNAs. *Nucleic Acids Res.* 2:1931–1939.
4. Söll, D. 1971. Enzymatic modification of transfer RNA. *Science*. 173: 293–298.
5. Okada, N., S. Noguchi, H. Kasai, N. Shindo-Okada, T. Ohgi, T. Goto, and S. Nishimura. 1979. Novel mechanism of post-transcriptional modification of tRNA. *J. Biol. Chem.* 254:3067–3073.
6. Bereswill, S., F. Faßbinder, C. Völzing, R. Haas, K. Reuter, R. Ficner, and M. Kist. 1997. Cloning and functional characterization of the genes encoding 3-dehydroquinate synthase (aroB) and tRNA-guanine transglycosylase (tgt) from *Helicobacter pylori*. *Med. Microbiol. Immunol.* 186:125–134.
7. Durand, J. M., N. Okada, T. Tobe, M. Watarai, I. Fukuda, T. Suzuki, N. Nakata, K. Komatsu, M. Yoshikawa, and C. Sasakawa. 1994. vacC, a virulence-associated chromosomal locus of *Shigella flexneri*, is homologous to tgt, a gene encoding tRNA-guanine transglycosylase (TGT) of *Escherichia coli* K-12. *J. Bacteriol.* 176:4627–4634.
8. Brenk, R., E. A. Meyer, K. Reuter, M. T. Stubbs, G. A. Garcia, F. Diederich, and G. Klebe. 2004. Crystallographic study of in transglycosylase suggests pharmacophore for virtual inhibitors of tRNA-guanine a new structure-based screening. *J. Mol. Biol.* 338:55–75.
9. Brenk, R., L. Naerum, U. Graedler, H.-D. Gerber, C. Sohn, G. A. Garcia, K. Reuter, M. T. Stubbs, and G. Klebe. 2003. Virtual screening for submicromolar lead inhibitors of TGT based on a new binding mode detected by crystal structure analysis. *J. Med. Chem.* 46:1133–1143.
10. Meyer, E. A., M. Furler, F. Diederich, R. Brenk, and G. Klebe. 2004. Synthesis and in vitro evaluation of 2-aminoquinazolin-4(3H)-one-based inhibitors for tRNA-Guanine transglycosylase (TGT). *Helv. Chim. Acta*. 87:1333–1356.
11. Grädler, U., R. Ficner, G. A. Garcia, M. T. Stubbs, G. Klebe, and K. Reuter. 1999. Mutagenesis and crystallographic studies of *Zymomonas mobilis* tRNA-guanine transglycosylase to elucidate the role of serine 103 for enzymatic activity. *FEBS Lett.* 454:142–146.
12. Kittendorf, J. D., L. M. Barcomb, S. T. Nonekowski, and G. A. Garcia. 2001. tRNA-guanine transglycosylase from *Escherichia coli*: molecular mechanism and role of aspartate 89. *Biochemistry*. 40:14123–14133.

13. Kittendorf, J. D., T. Sgraja, K. Reuter, G. Klebe, and G. A. Garcia. 2003. An essential role for aspartate 264 in catalysis by tRNA-guanine transglycosylase from *Escherichia coli*. *J. Biol. Chem.* 278:42369–42376.

14. Romier, C., K. Reuter, D. Suck, and R. Ficner. 1996. Mutagenesis and crystallographic studies of *Zymomonas mobilis* tRNA-guanine transglycosylase reveal aspartate 102 as the active site nucleophile. *Biochemistry.* 35:15734–15739.

15. Xie, W., X. J. Liu, and R. H. Huang. 2003. Chemical trapping and crystal structure of a catalytic tRNA guanine transglycosylase covalent intermediate. *Nat. Struct. Biol.* 10:781–788.

16. Romier, C., K. Reuter, D. Suck, and R. Ficner. 1996. Crystal structure of tRNA-guanine transglycosylase: RNA modification by base exchange. *EMBO J.* 15:2850–2857.

17. Goodenough-Lashua, D. M., and G. A. Garcia. 2003. tRNA-Guanine transglycosylase from *Escherichia coli*: a ping-pong kinetic mechanism is consistent with nucleophilic catalysis. *Bioorg. Chem.* 31:331–344.

18. Hansson, T., J. Marelius, and J. Åqvist. 1998. Ligand binding affinity prediction by linear interaction energy methods. *J. Comput. Aided Mol. Des.* 12:27–35.

19. Wang, J., R. Dixon, and P. A. Kollman. 1999. Ranking ligand binding affinities with avidin: a molecular dynamics-based interaction energy study. *Proteins.* 34:69–81.

20. Okada, N., and S. Nishimura. 1979. Isolation and characterization of a guanine insertion enzyme, a specific tRNA transglycosylase, from *Escherichia coli*. *J. Biol. Chem.* 254:3061–3066.

21. Gordon, A. J., and R. A. Ford. 1972. The Chemist's Companion: A Handbook of Practical Data, Techniques, and References. Wiley-Interscience, New York.

22. Harris, D. C. 1991. Quantitative Chemical Analysis. W. H. Freeman and Company, New York.

23. Leatherbarrow, R. 1990. GraFit Users Manual. Erithacus Software, Staines, U.K.

24. Cornell, W. D., P. Cieplak, C. I. Bayly, I. R. Gould, K. J. Merz, D. M. Ferguson, D. C. Spellmeyer, T. Fox, J. W. Caldwell, and P. A. Kollman. 1995. A second generation force field for the simulation of proteins, nucleic acids, and organic molecules. *J. Am. Chem. Soc.* 117: 5179–5197.

25. Chemical Computing Group. 1997. Molecular Operating Environment. Chemical Computing Group, Montreal, Canada.

26. Romier, C., J. E. W. Meyer, and D. Suck. 1997. Slight sequence variations of a common fold explain the substrate specificities of tRNA-guanine transglycosylases from the three kingdoms. *FEBS Lett.* 416:93–98.

27. Gilson, M. K. 1993. Multiple-site titration and molecular modeling: two rapid methods for computing energies and forces for ionizable groups in proteins. *Proteins.* 15:266–282.

28. Antosiewicz, J., J. A. McCammon, and M. K. Gilson. 1996. The determinants of pKas in proteins. *Biochemistry.* 35:7819–7833.

29. Carlson, H. A., J. M. Briggs, and J. A. McCammon. 1999. Calculation of the pKa values for the ligands and side chains of *Escherichia coli* Dalanine:D-alanine ligase. *J. Med. Chem.* 42:109–117.

30. Briggs, J. M., J. D. Madura, M. E. Davis, M. K. Gilson, J. Antosiewicz, B. A. Luty, R. C. Wade, B. Bagheri, A. Ilin, R. C. Tan, and J. A. McCammon. 1995. UHBD (University of Houston Brownian Dynamics), Version 5.1. University of California, San Diego.

31. Case, D. A., D. A. Pearlman, J. W. Caldwell, T. E. Cheatham III, W. S. Ross, C. L. Simmerling, T. A. Darden, K. J. Merz, R. V. Stanton, A. L. Cheng, J. J. Vincent, M. Crowley, V. Tsui, R. J. Radmer, Y. Duan, J. Pitera, I. Massova, G. L. Seibel, U. C. Singh, P. K. Weiner, and P. A. Kollman. 1999. AMBER 6, Version 6. University of California, San Francisco.

32. Pearlman, D. A., D. A. Case, J. W. Caldwell, W. S. Ross, T. E. Cheatham III, S. DeBolt, D. M. Ferguson, G. L. Seibel, and P. A. Kollman. 1995. AMBER, a package of computer programs for applying molecular mechanics, normal mode analysis, molecular dynamics and free energy calculations to simulate the structural and energetic properties of molecules. *Comput. Phys. Commun.* 91:1–41.

33. Åqvist, J., V. B. Luzhkov, and B. O. Brandsdal. 2002. Ligand binding affinities from MD simulations. *Acc. Chem. Res.* 35:358–365.

34. Åqvist, J., C. Medina, and J.-E. Samuelsson. 1994. A new method for predicting binding affinity in computer-aided drug design. *Protein Eng.* 7:385–391.

35. Wang, W., O. Donini, C. M. Reyes, and P. A. Kollman. 2001. Biomolecular simulations: recent developments in force fields, simulations of enzyme catalysis, protein-ligand, protein-protein, and protein-nucleic acid noncovalent interactions. *Annu. Rev. Biophys. Biomol. Struct.* 30:211–243.

36. Wang, W., J. Wang, and P. A. Kollman. 1999. What determines the van der Waals coefficient in the LIE (linear interaction energy) method to estimate binding free energies using molecular dynamics simulations? *Proteins.* 34:395–402.

37. Lamb, M. L., J. Tirado-Rives, and W. L. Jorgensen. 1999. Estimation of the binding affinities of FKBP12 inhibitors using a linear response method. *Bioorg. Med. Chem.* 7:851–860.

38. Smith, R. H., W. L. Jorgensen, J. Tirado-Rives, M. L. Lamb, P. A. Janssen, C. J. Michejda, and M. B. K. Smith. 1998. Prediction of binding affinities for TIBO inhibitors of HIV-1 reverse transcriptase using Monte Carlo simulations in a linear response method. *J. Med. Chem.* 41:5272–5286.

39. Barril, X., J. Gelpi, J. Lopez, M. Orozco, and F. Luque. 2001. How accurate can molecular dynamics/linear response and Poisson-Boltzmann/solvent accessible surface calculations be for predicting relative binding affinities? Acetylcholinesterase huprine inhibitors as a test case. *Theor. Chem. Acc.* 106:2–9.

40. Wall, I. D., A. R. Leach, D. W. Salt, M. G. Ford, and J. W. Essex. 1999. Binding constants of neuraminidase inhibitors: an investigation of the linear interaction energy method. *J. Med. Chem.* 42:5142–5152.

41. Hou, T. J., W. Zhang, and X. J. Xu. 2001. Binding affinities for a series of selective inhibitors of gelatinase-A using molecular dynamics with a linear interaction energy approach. *J. Phys. Chem. B.* 105:5304–5315.

42. Sham, Y., Z. Chu, H. Tao, and A. Warshel. 2000. Examining methods for calculations of binding free energies: LRA, LIE, PDLD-LRA, and PDLD/S-LRA calculations of ligands binding to HIV protease. *Proteins.* 39:393–407.

43. Marelius, J., K. Kolmodin, I. Feierberg, and J. Åqvist. 1998. Q: A molecular dynamics program for free energy calculations and empirical valence bond simulations in biomolecular systems. *J. Mol. Graph. Model.* 16:213–225.

44. Kittendorf, J. D. 2004. Catalysis by tRNA-guanine transglycosylase from *Escherichia coli*. PhD. thesis. University of Michigan, Ann Arbor.

45. Massova, I., and P. A. Kollman. 2000. Combined molecular mechanical and continuum solvent approach (MM-PBSA/GBSA) to predict ligand binding. *Perspect. Drug Discov. Des.* 18:113–135.

46. Bashford, D., and D. A. Case. 2000. Generalized born models of macromolecular solvation effects. *Annu. Rev. Phys. Chem.* 51:129–152.

47. Liu, H. Y., I. D. Kuntz, and X. Q. Zou. 2004. Pairwise GB/SA scoring function for structure-based drug design. *J. Phys. Chem. B.* 108:5453–5462.

48. Baker, N. A. 2004. Poisson-Boltzmann methods for biomolecular electrostatics. *Methods Enzymol.* 383:94–118.

49. Ishitani, R., O. Nureki, S. Fukai, T. Kijimoto, N. Nameki, M. Watanabe, H. Kondo, M. Sekine, N. Okada, S. Nishimura, and S. Yokoyama. 2002. Crystal structure of archaeosine tRNA-guanine transglycosylase. *J. Mol. Biol.* 318:665–677.

50. Canyuk, B., P. J. Focia, and A. E. Eakin. 2001. The role for an invariant aspartic acid in hypoxanthine phosphoribosyltransferases is examined using saturation mutagenesis, functional analysis, and x-ray crystallography. *Biochemistry.* 40:2754–2765.

51. Reuter, K., S. Chong, F. Ullrich, H. Kersten, and G. A. Garcia. 1994. Serine-90 is required for enzymic activity by tRNA-guanine transglycosylase from *Escherichia coli*. *Biochemistry*. 33:7041–7046.

52. Grädler, U., H. D. Gerber, D. M. Goodenough-Lashua, G. A. Garcia, R. Ficner, K. Reuter, M. T. Stubbs, and G. Klebe. 2001. A new target for shigellosis: rational design and crystallographic studies of inhibitors of tRNA-guanine transglycosylase. *J. Mol. Biol.* 306:455–467.

53. Brenk, R., M. T. Stubbs, A. Heine, K. Reuter, and G. Klebe. 2003. Flexible adaptations in the structure of the tRNA-modifying enzyme tRNA-guanine transglycosylase and their implications for substrate selectivity, reaction mechanism and structure-based drug design. *ChemBioChem*. 4:1066–1077.

54. Goodenough-Lashua, D. M. 2002. Mechanistic studies of the reaction catalyzed by eubacterial tRNA guanine transglycosylase. PhD. thesis. University of Michigan, Ann Arbor. 182.